Hadron production in non linear relativistic mean field models

M. Chiapparini,[1,*] M. E. Bracco,[2] A. Delfino,[3] M. Malheiro,[4] D. P. Menezes,[5] and C. Providência[6]

[1]*Instituto de Física, Universidade do Estado do Rio de Janeiro, Rua São Francisco Xavier 524, Maracanã, CEP 20550-900 Rio de Janeiro, RJ, Brazil.*

[2]*Faculdade de Tecnologia, Universidade do Estado do Rio de Janeiro, Rodovia Presidente Dutra km 298, Pólo Industrial, CEP 27537-000, Resende, RJ, Brazil.*

[3]*Instituto de Física, Universidade Federal Fluminense, Av. Gal. Milton Tavares de Souza s/n°., Gragoatá, CEP 24210-346 Niterói, RJ, Brazil.*

[4]*Instituto Tecnológico da Aeronáutica, Praça Marechal Eduardo Gomes 50, Vila das Acácias, CEP 12228-900 São José dos Campos, SP, Brazil.*

[5]*Depto de Física, CFM, Universidade Federal de Santa Catarina, CP. 476, CEP 88040-900 Florianópolis, SC, Brazil.*

[6]*Centro de Física Computacional, Dep. de Física, Universidade de Coimbra, P-3004 - 516, Coimbra, Portugal.*

Abstract

By using a parametrization of the non-linear Walecka model which takes into account the binding energy of different hyperons, we present a study of particle production yields measured in central Au-Au collision at RHIC. Two sets of different hyperon-meson coupling constants are employed in obtaining the hadron production and chemical freeze-out parameters. These quantities show a weak dependence on the used hyperon-meson couplings. Results are in good overall accordance with experimental data. We have found that the repulsion among the baryons is quite small and, through a preliminary analysis of the effective mesonic masses, we suggest a way to improve the fittings.

PACS numbers: 21.65.-f,24.10.Jv,25.75.-q

*Electronic address: chiappa@uerj.br

I. INTRODUCTION

Lattice simulations of QCD indicate that, at zero baryon number density and temperatures of the order of 150-170 MeV, quarks and gluons become deconfined [1, 2, 3]. This novel phase of nuclear matter is commonly called quark-gluon plasma (QGP). It is believed that in nature temperatures of the order of 150 MeV existed only shortly after the Big Bang. For more than two decades, attempts have been made to recreate similar conditions within the collision of heavy nuclei at ultra-relativistic energies, looking for signatures of the production of the QGP, which subsequently hadronizes. The hadronization stage has been well discussed in the literature [4]. After this process takes place, one assumes that a hadronic gas appears in a sizeable region of space. Hydrodynamic models were used to describe this hadronic evolution, based on the hypothesis that the fireball size is large in comparison with the mean free path of the hadrons [5, 6]. One may ask whether the hydrodynamic approach needs to consider viscosity and heat conduction effects, even before the freeze-out occurs. Here, one must say that the employment of any kind of model has to be taken with caution. In the gas regime, and for temperatures far from the system critical temperature, the relaxation times which control the chemical equilibrium of hadrons may become large compared with collision times, causing the gas to reach the chemical equilibrium at an early stage of the expansion, favoring an overpopulation of pions [7]. Temperature and chemical potential are related to the chemical freeze-out regime. At low beam energies the chemical freeze-out of the resulting gas may be described by low temperature and high baryonic chemical potential. As the beam energy increases this situation reverts. The mesons become more numerous, the temperature increases and the chemical baryonic potential decreases. For small baryonic chemical potential and high temperature the number of baryons becomes close to the anti-baryons. Within this scenario, a QGP-hadronic matter phase transition is probably going to happen in heavy-ion collisions at very high energy, as the ones extected to take place soon at the Large Hadron Collider (LHC/ALICE).

Hadron multiplicities are observables which can provide valuable information on the nature of the medium from which they are produced. In this way, they are natural tools to look for QGP signatures. Different models have been used to improve the understanding of the QGP-hadronic matter phase transition [8, 9, 10, 11, 12]. The use of thermal models to describe hadronic collision spectra has also been considered [13, 14]. Curiously, despite

the fact that no microscopic theoretical basis was given for thermalization in such collisions, these models have been quite successful.

In thermal models, the statistical distribution is controlled basically by the temperature and the chemical potential of a free hadron-gas. However, these ingredients alone does not suffice since without a repulsion dynamics, the gas does not expand properly. Therefore, for baryons and mesons, an excluded volume is needed in the same spirit as in a Van der Waals gas. In particular, a detailed explanation of how incorporate a thermodynamically consistent excluded volume effect in a hadron gas was presented in [15, 16]. The excluded volume parameters are determined according to the fits of heavy-ion collision data. To fit Au-Au and Pb-Pb hadronic ratios data [13, 14, 17], a common hard-core for baryons and mesons suffices.

In a different approach, that does not consider any correlation between baryons, an interesting work [18] has shown that the energy per baryon remains almost constant and equal to 1 GeV in a broad range of chemical freeze-out temperatures.

More recently, studies including hadron-hadron dynamics in a sophisticated relativistic chiral SU(3) model, have shown that the hadron ratios obtained from SIS, AGS, SPS to RHIC hadron energies are also well described [19]. This calculation, contrary to thermal models, takes into account in medium hadronic mass effects. This new ingredient appears to modify substantially the temperature and the baryonic chemical potential to the freeze-out fittings. This happens even when the SU(3) models are undergoing a first or a second order phase transition. As a side information, let us remark that a first order phase transition in a hadronic model induces a dramatic decrease in the effective baryonic masses as well as a discontinuity in the entropy. In the SU(3) model, both mesonic and baryonic masses are obtained with in medium effects.

Between the simplicity of the thermal models [13, 14, 17] and the complexity of the relativistic chiral SU(3) model [19], one would ask whether well known relativistic hadronic models [20, 21] are able to successfully fit the mentioned chemical freeze-out hadronic ratios. In a previous study [22] the antibaryon ($\bar{p}, \bar{\Lambda}$) production in relativistic nuclear collisions using nonlinear models has been presented. The authors estimated the ratio of antibaryon and baryon densities in interacting and in free systems. It was also pointed out that the annihilation of antibaryons in surrounding matter at the final stage of the reaction may reduce their abundancy [22]. Relativistic hadronic models are based on field theories describing

nuclear matter as a strongly interacting system of baryons and mesons. This approach is assumed to be valid below the deconfinement phase transition, and is based on the identification of the appropriate degrees of freedom at this scale. The prototype of such theory is Quantum Hadrodynamics (QHD) [20, 21], which has been shown to describe well many properties of nuclear matter, finite nuclei and neutron stars [20, 21, 23, 24, 25, 26, 27]. This theory can be extended to include many-body correlations as density-dependent meson couplings [28, 29]. The successful description of nuclear properties indicates that the essential aspects of low energy strong interactions are well described by QHD. At high energy, it can describe dynamically the evolution from the hadronic fireball starting scenario to the chemical freeze-out in which the baryons and the light mesons populate the gas. One of the advantages of using relativistic quantum-hadronic models is that they can also describe the already mentioned QGP-hadronic matter phase transition as the chemical potential increases [11, 12]. The physics of the hadronic models at high temperature is very rich and its behavior has been well investigated for zero chemical potential [30]. Depending on their parametrization, the models can present a first or second order phase transition in the same way as the already mentioned SU(3) model for the hadronic masses.

It is natural then to ask whether these routinely used relativistic hadronic models can describe the hadron production observed today in Au-Au collisions at RHIC [14]. Recently, some of these models, with and without density depend hadron-meson coupling constants, have been used in order to answer that question [31]. In that calculation not only the baryonic octet was included but also the decuplet. A good overall description of the particle yields data was obtained and in particular for K^{0*}/h^- and $\bar{K}^{0*}/h^-$ ratios, a good improvement was achieved in comparison with the results obtained in the free gas approximation [14]. In [31] it was shown that the new dynamics achieved by the models with density depend parameters makes the difference by having the best fits and that the mesons play an important role. To go further with this investigation, we have chosen to consider in the present work only the baryonic octet because the inclusion of the decuplet produced only a small change in the overall results. Moreover, we take into account the different binding energies of the hyperons [32, 33, 34, 35] in obtaining the chemical freeze-out parameters. We also restrict ourselves to one parametrization of the non-linear Walecka model [20, 21, 23, 24].

In order to investigate the role played by the mesons, we have introduced, in a very crude and naive way, an *ad-hoc* effective mesonic mass m^* that increases in the medium and obeys

a universal scaling with its bare value: $m^*/m = \alpha$, $\alpha > 1$, for all mesons. Using a best fitting analysis, we established a correlation between the χ^2 per degree of freedom (χ^2_{dof}) and α, understanding the result as an indication that the increase of the in-medium meson masses introduces additional repulsion among the particles and mimics the repulsive effect obtained in other approaches, where the hadron excluded volume is taken into account [13, 14].

The paper is organized as follows. In Sec. II we present the models with a detailed discussion on chemical, strangeness and charge equilibrium. In Sec. III, we present the parametrizations used for the couplings between hyperons and mesons. In Sec. IV, we present our results and summarize our main conclusions.

II. THE MODEL

We assume that the chemical freeze-out can be described as a mixture of the lightest baryons and mesons. We use the following Lagrangian

$$\mathcal{L} = \mathcal{L}_{QHD} + \mathcal{L}_{\pi K\rho}, \tag{1}$$

where

$$\mathcal{L}_{QHD} = \mathcal{L}_b + \mathcal{L}_m, \tag{2}$$

with

$$\begin{aligned}
\mathcal{L}_b &= \sum_j \bar{\psi}_j \left\{ \gamma_\mu \left[i\partial^\mu - g_{\omega j}\omega^\mu - g_{\rho j} I_{3j} \rho^{0\mu} \right] - (m_j - g_{\sigma j}\sigma) \right\} \psi_j, \\
\mathcal{L}_m &= \frac{1}{2}\left(\partial_\mu\sigma\partial^\mu\sigma - m_\sigma^2\sigma^2\right) - \frac{b}{3}\left(g_{\sigma N}\sigma\right)^3 - \frac{c}{4}\left(g_{\sigma N}\sigma\right)^4 - \frac{1}{4}\left(\partial_\mu\omega_\nu - \partial_\nu\omega_\mu\right)^2 \\
&\quad + \frac{1}{2}m_\omega^2\omega_\mu\omega^\mu - \frac{1}{4}\left(\partial_\mu\rho_\nu^0 - \partial_\nu\rho_\mu^0\right)^2 + \frac{1}{2}m_\rho^2\rho_\mu^0\rho^{0\mu}.
\end{aligned} \tag{3}$$

Mesons $\{\pi^\pm, K^0, \bar{K^0}, K^\pm, \rho^\pm, K^{*0}, \bar{K^{*0}}, K^{*\pm}\}$ enter Lagrangian $\mathcal{L}_{\pi K\rho}$ in (1) as a free gas of bosons. Lagrangian (2) has a general form commonly used in relativistic mean field models. The sum over j in (3) extends over the octet of lightest baryons $\{n, p, \Lambda, \Sigma^-, \Sigma^0, \Sigma^+, \Xi^-, \Xi^0\}$, and their antiparticles. I_{3j} is the corresponding isospin quantum number. The baryon and meson masses are listed in Table I. The values for the couplings are taken from [26] and shown in Table II. The Euler-Lagrange equations of motion for the mediating mesons in a system with translational and rotational invariance, within the mean field approximation,

	N	Λ	Σ	Ξ	π	K	ρ	K^*
m (MeV)	939	1116	1193	1318	138	495	776	893

TABLE I: Masses used in the calculation.

K (MeV)	m^*/m	l_σ (fm^{-2})	l_ω (fm^{-2})	l_ρ (fm^{-2})	b (fm^{-1})	c
300	0.70	11.79	7.149	4.411	0.01402	-0.001070

TABLE II: Parameters used in the calculation ($l_i = g_{iN}^2/m_i^2$), taken from Ref. [26] (b here includes the product with m_N in Eq. (1) of this reference).

are

$$V_\sigma = l_\sigma \left(\sum_j x_{\sigma j} n_{sj} - b V_\sigma^2 - \mathrm{c} V_\sigma^3 \right), \tag{4}$$

$$V_\omega = l_\omega \sum_j x_{\omega j} n_j, \tag{5}$$

$$V_\rho = l_\rho \sum_j x_{\rho j} n_{3j}, \tag{6}$$

with $V_\sigma = g_{\sigma N}\sigma$, $V_\omega = g_{\omega N}\omega_0$, $V_\rho = g_{\rho N}\rho_0^0$, $x_{ij} = g_{ij}/g_{iN}$ and $l_i = g_{iN}^2/m_i^2$, $\;i = \sigma, \omega, \rho$. The densities entering the above equations are

$$n_{sj} = \frac{1}{\pi^2} \int \frac{m_j^*}{\epsilon_j(p)} (f_{j+} + f_{j-}) p^2 dp, \tag{7}$$

$$n_j = \frac{1}{\pi^2} \int (f_{j+} - f_{j-}) p^2 dp, \tag{8}$$

$$n_{3j} = I_{3j} n_j, \tag{9}$$

where $m_j^* = m_j - g_{\sigma j}\sigma$ is the effective mass of the baryon j, and $\epsilon_j(p) = \sqrt{p^2 + m_j^{*2}}$. The baryonic distribution functions $f_{j\pm}$ are the Fermi-Dirac ones

$$f_{j\pm} = \frac{1}{\exp\left[(\epsilon_j \mp \nu_j)/T\right] + 1}, \tag{10}$$

where the sign minus (plus) accounts for particles (antiparticles). The baryonic effective chemical potential ν_j is defined as

$$\nu_j = \mu_j - g_{\omega j}\omega_0 - g_{\rho j} I_{3j} \rho_0^0, \tag{11}$$

being μ_j the thermodynamical chemical potential of baryon j. The particle density of the free mesons π, K, ρ and K^* are calculated using the Bose-Einstein distribution function in the form

$$n_l = \frac{\gamma_l}{2\pi^2} \int \frac{1}{\exp\left[(\epsilon_l - \mu_l)/T\right] - 1} p^2 dp, \quad l = \pi, K, \rho, K^* \tag{12}$$

where $\epsilon_l = \sqrt{p^2 + m_l^2}$, μ_l is the chemical potential, and γ_l is the corresponding spin degeneracy.

The problem is solved in the grand canonical ensemble, imposing the constraints of baryon number, strangeness and electric charge conservation, given respectively by [13]:

$$V \sum_i n_i B_i \;=\; Q_B = Z + N, \tag{13}$$

$$V \sum_i n_i S_i \;=\; Q_S = 0, \tag{14}$$

$$V \sum_i n_i I_{3i} \;=\; Q_{I_3} = (Z - N)/2, \tag{15}$$

where i runs over all particles in the system, and $\{B_i, S_i, I_{3i}\}$ are the baryonic, strangeness and isospin quantum numbers of particle i. Each conserved charge has a conjugated chemical potential, namely $\{Q_B, Q_S, Q_{I_3}\} \leftrightarrow \{\mu_B, \mu_S, \mu_{I_3}\}$. The temperature T and the baryochemical potential μ_B are the two independent parameters of the model, while the volume of the fireball V, the strangeness chemical potential μ_S, and the isospin chemical potential μ_{I_3} are fixed by the three constraints (13)-(15). The chemical potential of each particle in the system can be written as a linear combination of these three conjugate chemical potentials in the form

$$\mu_i = B_i \mu_B + I_{3i} \mu_{I_3} + S_i \mu_S. \tag{16}$$

In the baryonic sector, a zero chemical potential implies a zero baryonic density since the number of baryons is equal to the anti-baryons. For the π^0, for instance, zero chemical potential is obtained directly from Eq. (16), using $B_{\pi^0} = I_{3\pi^0} = S_{\pi^0} = 0$. Despite the fact that $\mu_{\pi^0} = 0$, the density for π^0 is different from zero. This remark applies only to π^0 and ρ^0. In particular, π^0 results completely decoupled from the other particles. Its population is that of a boson gas at temperature T and zero chemical potential. This is the reason why it was not considered in Lagrangian $\mathcal{L}_{\pi K \rho}$ in (1). Consistently, particle ratios do not involve the π^0 and ρ^0 mesons [14]. Hence, these particles do not need to be considered in the equations of the chemical potentials. Note that the ρ^0 meson appears in Lagrangian $\mathcal{L}_m$, Eq. (3), only as a mediating field in the mean field approximation.

In the bosonic sector, the chemical potentials have to obey the physical inequality,

$$\mu_l \leq m_l, \tag{17}$$

where m_l is the bosonic mass. This constraint is imposed naturally by statistical mechanics in order to keep the bosonic partition function finite.

The constraints contained in Eqs.(16,17) allow us to restrict the possible values of the generalized chemical potentials by the following inequalities:

$$0 \leq |\mu_{I_3}| \leq m_\pi, \tag{18}$$

$$0 \leq |\mu_S| \leq -\frac{1}{2}|\mu_{I_3}| + m_K. \tag{19}$$

This set of inequalities was implemented numerically in order to solve the large self-consistent set of equations of the problem.

III. THE HYPERONIC COUPLINGS

The coupling constants of the hyperons to the ω and ρ mesons are fixed using SU(6) symmetry [35], which means that the vector coupling constants scale with the number of light quarks in the baryon in the form $g_{\omega N} : g_{\omega\Lambda} : g_{\omega\Sigma} : g_{\omega\Xi} = 3 : 2 : 2 : 1$. The ratios of the vector couplings are then fixed to

$$x_{\omega\Lambda} = x_{\omega\Sigma} = \frac{2}{3}, \qquad x_{\omega\Xi} = \frac{1}{3}, \tag{20}$$

meaning that the vector coupling constants of the hyperonic sector are fixed once the $g_{\omega N}$ coupling constant is know.

The coupling strength of the ρ meson, however, is given by the isospin of the baryon in the form $g_{\rho N} : g_{\rho\Lambda} : g_{\rho\Sigma} : g_{\rho\Xi} = 1/2 : 0 : 1 : 1/2$. Again, the isovector coupling constants of the hyperonic sector are fixed once $g_{\rho N}$ is know. This is taken into account automatically with the specific form of the isovector couplings in Lagrangian (3) choosing

$$x_{\rho i} = 1, \qquad i = \Lambda, \Sigma, \Xi. \tag{21}$$

The coupling constants $\{x_{\sigma i}\}_{i=\Lambda,\Sigma,\Xi}$ of the hyperons with the scalar meson σ are constrained by the hypernuclear potentials in nuclear matter to be consistent with hypernuclear data [32, 33, 34]. The hypernuclear potentials were constructed as

$$V_i = x_{\omega i} V_{\omega N} - x_{\sigma i} V_{\sigma N}, \qquad i = \Lambda, \Sigma, \Xi, \tag{22}$$

	$x_{\omega\Lambda}$	$x_{\omega\Sigma}$	$x_{\omega\Xi}$	$x_{\sigma\Lambda}$	$x_{\sigma\Sigma}$	$x_{\sigma\Xi}$	$x_{\rho i}$
Set1	0.6666	0.6666	0.6666	0.6104	0.6104	0.6104	0.6104
Set2	0.6666	0.6666	0.3333	0.6106	0.4046	0.3195	1.000

TABLE III: Parametrizations used for the hyperon coupling constants. Set1 is taken from Ref. [26]. Set2 is obtained from Set1 imposing SU(6) symmetry and different binding energies for hyperons in nuclear matter (see text for details). The last column, $x_{\rho i}$, refers to the coupling of the ρ meson with all hyperons, $i = \Lambda, \Sigma, \Xi$.

where $V_{\omega N} = 215.83$ MeV and $V_{\sigma N} = 281.47$ MeV are the nuclear potentials for symmetric nuclear matter at saturation with the parameters of Table II. Following Ref. [33] we use

$$V_\Lambda = -28 \text{ MeV}, \qquad V_\Sigma = 30 \text{ MeV}, \qquad V_\Xi = -18 \text{ MeV}. \tag{23}$$

All hyperon coupling ratios $\{x_{\sigma i}, x_{\omega i}, x_{\rho i}\}_{i=\Lambda,\Sigma,\Xi}$ are now known once the coupling constants $\{g_{\sigma N}, g_{\omega N}, g_{\rho N}\}$ of the nucleon sector are given.

We have to guarantee also that the hyperon coupling ratios are constrained to the known neutron star maximum masses, as in Ref. [26]. In this reference windows are established for the values of x_σ and x_ω: x_σ and x_ω are the couplings between hyperons and σ and ω meson respectively and they have to be compatible with the allowed maximum neutron star masses and with the Λ binding energy in nuclear matter. Couplings x_σ and x_ω are the same for all hyperons and the x_ρ couplings are fixed arbitrarily as $x_\rho = x_\sigma$. The SU(6) value $x_\omega = 2/3$ of Eq.(20) together with $x_\sigma = 0.6104$, is one of the allowed couple of values (they were interpolated from Table I of Ref. [26]). This choice corresponds to Set1 row in Table III. The other couplings used in Ref. [26] are those shown in Table II. Through this work we refer to this relativistic model as GM1. Now we modify Set1 to take into account constraints (20)-(23). The value $x_{\omega\Lambda} = 2/3$ is kept constant and the others are modified accordingly with the constraints. The resulting set of hyperonic couplings is the Set2 row in Table III.

To see the impact of this redefinition of hyperonic couplings on neutron star properties, we show in Fig. 1 the equations of state calculated using the model of Ref. [26] with Set1 (dashed line) and with Set2 (full line) of Table III for the hyperon coupling constants. As we can see, both curves are almost indistinguishable, ensuring the same neutron star properties.

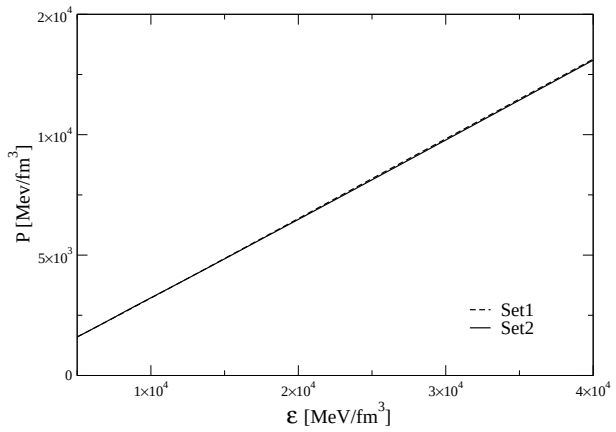

FIG. 1: Equations of state for the relativistic models of Ref. [26] (dashed line, Set1 in Table III) and the one of this work (full line, Set2 in Table III). Both equations of state are almost indistinguishable, ensuring the same neutron-star maximun masses.

This validates Set2 as a set of hyperonic couplings that preserves maximum neutron star masses as well as experimental results for the binding energy of hyperons in symmetric nuclear matter. In the following, we use Set1 and Set2 for the hyperonic couplings in the Lagrangian (1) together with parameters of Table II to investigate particle production in relativistic heavy ion collisions.

IV. RESULTS AND CONCLUSIONS

We apply the above formalism to the description of the experimental data for hadron production yield in Au-Au collisions at RHIC from STAR, PHENIX, PHOBOS and BRAHMS collaborations, following [14] and references therein. We adjust the free parameters T and μ_B to get the best description of the data, based on a χ^2 analysis of the form [13]

$$\chi^2 = \sum_i \left(\frac{R_i^{exp.} - R_i^{mod.}}{\sigma_i} \right)^2 , \tag{24}$$

where $R_i^{mod.}$ is the ith particle ratio obtained from the models used here and σ_i is the experimental error. When more than one experimental data is available, we calculated a weighted average. This leaves us with seven effective degrees of freedom for the fit.

Our results are summarized in Table IV for the hyperon coupling constants given in Table III. We also show, in the fourth column, the results from a non-interacting gas of baryons

	GM1		Free	Free*	Th	Exp. Data	Exp.
Ratio	Set1	Set2					
$\bar{p}/p$	0.673	0.676	0.674	0.638	0.629	0.65±0.07	STAR
						0.64±0.07	PHENIX
						0.60±0.07	PHOBOS
						0.64±0.07	BRAHMS
$\bar{p}/\pi^-$	0.048	0.046	0.038	0.080	0.078	0.08±0.01	STAR
π^-/π^+	1.005	1.005	1.004	1.011	1.007	1.00±0.02	PHOBOS
						0.95±0.06	BRAHMS
K^-/K^+	0.957	0.959	0.964	0.888	0.894	0.88±0.05	STAR
						0.78±0.13	PHENIX
						0.91±0.09	PHOBOS
						0.89±0.07	BRAHMS
K^-/π^-	0.239	0.237	0.231	0.175	0.145	0.149±0.02	STAR
K^{*0}/h^-	0.063	0.062	0.059	0.038	0.037	0.06±0.017	STAR
$\bar{K^{*0}}/h^-$	0.060	0.059	0.057	0.033	0.032	0.058±0.017	STAR
$\bar{\Lambda}/\Lambda$	0.692	0.694	0.699	0.717	0.753	0.77±0.07	STAR
Ξ^+/Ξ^-	0.723	0.713	0.725	0.806	0.894	0.82±0.08	STAR
T (MeV)	148.6	148.0	145.7	169.4	174		
μ_B (MeV)	33.27	32.51	28.88	38.52	46		
χ^2_{dof}	5.65	5.77	6.24	1.08	0.81		

TABLE IV: Comparisons of experimental particle ratios with the ones obtained from the relativistic mean-field models used in this work for the hyperon couplings belonging to Set1 and Set2 , together with the chemical freeze-out temperature T, baryonic potential μ_B and χ^2_{dof}. Also shown are the results from the free gas (Free), from the free gas with *ad-hoc* effective meson masses (Free*, $m^*/m = 1.3$), and from the thermal model of [14] (Th). Experimental values of Au-Au collisions at $\sqrt{s} = 130$ MeV were taken from that reference and references therein.

and mesons (Free), in the fifth column the results from a non-interacting gas of baryons and mesons with effective meson masses as discussed below (Free*), together with the results from the thermal model of Ref. [14] in column six (Th).

We can see that both set of hyperonic couplings give almost the same results for the particle ratios. They are not very different from the model with zero coupling constants designated by Free, although in this case a smaller temperature and chemical potential were obtained. As a whole the fractions are well described, but we observe that there is a systematic deviation for the fractions involving mesons except for π^-/π^+. This reflects the naive way the mesons were included. However, we point out that the K^{*0}/h^- and $\bar{K^{*0}}/h^-$ ratios have improved with respect to the thermal model results in accordance with our previous work [31] and also with the chiral SU(3) calculations [19]. For h^- we designated all negatively charged hadrons produced, including mesons and baryons.

Regarding the quality of the fit, the resulting χ^2_{dof} for both sets are around 5.70, showing a slight improvement of Set1 over Set2 . When these values are multiplied by the seven degrees of freedom used in our fitting, χ^2 reaches 40, which is a high value. This does not happen with the fits obtained by thermal models [13, 14, 17] and with the chiral SU(3) model [19], for which χ^2 is around 6.

Looking now at the freeze-out temperatures, we see that they are almost the same for the two sets of hyperonic couplings considered ($T = 148.6 - 148.0$ MeV), showing a small decrease when going from Set1 to Set2 . This situation repeats for the chemical potential fitting ($\mu = 33.27 - 32.51$ MeV). It is important to mention at this point that in these models the hadronic phase transition regions occur at temperatures $T > 180$ MeV [12], higher than the freeze-out temperature we found here.

In order to better understand why we obtain a high χ^2_{dof}, we argue that the repulsion among the baryons is quite small and cannot describe so well the chemical freeze-out environment. This happens because the chemical potential is too low in comparison with the temperature. The other cited approaches certainly have sufficient built in repulsion to avoid an overpopulation of particles. In the thermal model, it is done through excluded volumes introduced in a thermodynamically consistent way. On the other hand, the chiral SU(3) model includes meson-meson and meson-baryon interactions, providing effective masses for all hadrons, giving a higher kinetic energy which mimics an additional repulsion among the particles.

We think that the relativistic models themselves suffer from a lack of repulsive correlations at low densities, where the sources for the mediating meson fields are very weak. For example, in the GM1 model with Set2 , studied in this work, we have $V_{\sigma N} = 21.44$ MeV, $V_{\omega N} = 3.359$ MeV, and $V_{\rho N} = -0.8919 \times 10^{-2}$ MeV. This fact results in a system almost identical to the one described by a free gas of baryons and mesons, as we can see comparing columns 2, 3 and 4 in Table IV. Therefore, the hadron production is not very sensitive to the hadron-meson interactions, manifested in the almost model independence of the χ^2_{dof} obtained and also in the small dependence of the freeze-out parameters. In spite of the reduced number of models studied here, the results obtained in [31], where more models were considered, also reinforce this point. This conjecture may be extended to all relativistic hadronic models commonly used in the literature.

Understanding the reason underlying the lack of repulsion in the description of the chemical freeze-out regime is a relevant question. In the following, we present a crude argument for that. Let us suppose, for simplicity, that baryon-baryon interaction proceeds through an attractive scalar (S) and a repulsive vector (V) meson-exchange potentials. In the mean field approach, at zero temperature and at normal saturated nuclear matter, the depth of $\Sigma = S + V$ is around 60 MeV. The temperature increase in these models favors the appearance of anti-baryons. Table IV shows that the $\bar{p}/p$ ratio is around 0.67. However, from G-parity symmetry, the anti-baryons themselves revert the sign of the vector potential in such a way that $\Sigma = S - V$ [36, 37, 38]. Thus, anti-baryon-baryon interactions themselves do not carry repulsion. Therefore, the baryon-baryon repulsion alone has to compensate for the large attraction among the anti-baryons, explaining the lack of repulsion in the hadronic models.

One way of implementing a repulsive content in this class of hadronic models would be by introducing an excluded volume for the particles in the system [15, 16, 39]. Of course, this approach requires the recalculation of the coupling constants in order to maintain the correct normal nuclear matter properties of the original models. By doing so, however, the hadronic models would loose its strong appealing due to their theoretical basis together with the success in reproducing so many observables in several different regimes of nuclear matter. Another possibility, inspired by the SU(3) hadronic model [19], is to include meson-meson self-coupling and meson-baryon couplings for the heavy mesonic sector, as K and ρ for example. We have studied this effect in an *ad-hoc* and crude way. In the statistical thermal

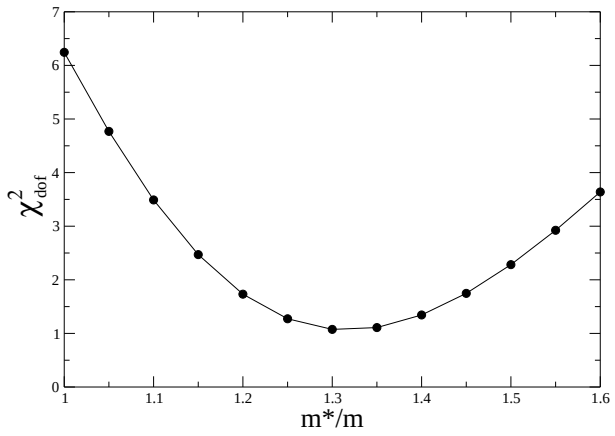

FIG. 2: χ^2_{dof} as a function of m^*/m (the same for all mesons), where m is the meson bare mass, for a free relativistic gas of baryons and mesons (baryon masses are mantained fixed to the experimental values of Table I).

distributions of the free gas, we have artificially assumed in-medium effective mesonic masses m^*, instead of the bare ones in vacuum. In this preliminary study, we have used the same value of m^*/m for all mesons. In Figure 2 we see how χ^2_{dof} becomes smaller as m^*/m increases from 1, reaches a minimum around $m^*/m \approx 1.3$, and starts to grow again. This shows that an increase in the effective in-medium mesonic mass goes in the right direction towards obtaining a better fit of the data. This is confirmed looking at column 5 in Table IV, where the particle ratios for $m^*/m = 1.3$, close to the minimum of Fig. 2, are shown. The increase of the in-medium meson masses would be compatible with the notion of a thermal mass which increases linearly with temperature. This kind of behaviour can be seen in chiral effective models [19] and also in the Walecka model [40]. Including the effective meson masses in this *ad-hoc* way, we automatically improve the ratios involving mesons, and reduce the fractions involving h^-. We point out, however, that in fact the uncertainty on the measured values of K^{*0}/h^- and $\bar{K}^{*0}/h^-$ are quite large. Also, the equilibrium temperatures increases more than 15% and the chemical potential 33%, coming closer to the results of the thermal model.

This finding strongly suggests that introducing an appropriate dynamic treatment of the mesons, allowing for the modification of their masses in medium, would favor the correct data ratios without the need of including excluded volumes. However, the model dependence addressed in Ref. [19] remains to be further investigated.

Another remark regards the particle ratios in the medium as we have calculated and the ones measured. The later comes from asymptotic particle states with vaccuum masses, i.e., on the mass shell ($m^* = m$). In our model calculation the particles are off-shell and any mechanism to bring them on-shell would modify the ratios. However, we did not include annihilation and nonequilibrium processes which are claimed to reduce the calculated yields [22].

Summarizing, in this work we have investigated the effects of different hyperon-meson coupling constants in hadron production and chemical freeze-out parameters. We have observed that the freeze-out temperatures and chemical potentials show a small dependence on the different parametrizations. Our results indicate that the repulsion among the baryons is quite small and the hadron production is not very sensitive to the hadron-meson interactions. A simple *ad hoc* in-medium mesonic mass study shows the importance of having meson-meson interaction in the hadronic models.

Acknowledgments

This work was partially supported by CNPq (Brazil) and FEDER/FCT (Portugal) under the project PTDC/FIS/64707/2006. Two of the authors (M.C. and M.E.B.) would like to thank Prof. Marcelo Munhoz for valuable discussions.

[1] Z. Fodor and S.D. Katz, JHEP0404 (2004) 50.

[2] F. Karsch, Nucl. Phys. B83,84 (Proc. Suppl.) (2000) 14.

[3] P. Petreczky et al, Nucl. Phys. A698 (2002) 400.

[4] U. Heinz, K. S. Lee and E. Schnedermann, Quark-gluon Plasma in Advanced Series on Directions in High Energy Physics, vol. 6 (World Scientific, Singapore, 1990).

[5] G. Baym, B. L. Friman, J. P. Blaizot, M. Soyeur and W. Czys, Nucl. Phys. A407 (1983) 541.

[6] U. Ornik, F. Pottag and R. M. Weiner, Phys. Rev. Lett. 63 (1989) 2641.

[7] H. Bebie, P. Gerber, J. L. Goity and H. Leutwyler, Nucl. Phys. B378 (1992) 95.

[8] G. E. Brown and M. Rho, Phys. Rep. 269 (1996) 333.

[9] U. Heinz, P. R. Subramanian, H. Stöcker and W. Greiner, J. Phys. G: Nucl. Part. Phys. 12 (1986) 1237.

[10] Bo-Qiang Ma, Qi-Ren Zhang, D. H. Rischke and W. Greiner, Phys. Lett. B315 (1993) 29.

[11] A. Delfino, M. Chiapparini, M. E. Bracco, L. Castro and S. E. Epsztein, J. Phys. G: Nucl. Part. Phys. 27 (2001) 2251.

[12] A. Delfino, J. B. Silva, M. Malheiro, M. Chiapparini and M. E. Bracco, J. Phys. G: Nucl. Part. Phys. 28 (2002) 2249.

[13] P. Braun-Munzinger, I. Heppe and J. Stachel, Phys. Lett. B465 (1999) 15.

[14] P. Braun-Munzinger, D. Magestro, K. Redlich and J. Stachel, Phys. Lett. B518 (2001) 21.

[15] D. H. Rischke, M. I. Gorenstein, H. Stöcker, and W. Greiner, Z. Phys. C51 (1991) 485

[16] D. Y. Granddon, M. I. Gorenstein, W. Greiner, and S. N. Yang, Phys. Rev. C56 (1997) 2210.

[17] F. Becattini and L. Ferroni, Eur. Phys. J. C38 (2004) 225.

[18] J. Cleymans and H. Satz, Z. Phys. C57 (1993) 135.

[19] D. Zschiesche, S. Schramm, J. Schaffner-Bielich, H. Stöcker and W. Greiner, Phys. Lett. B547 (2002) 7.

[20] J.D. Walecka, Ann. Phys. 83 (1974) 497.

[21] B.D. Serot and J.D. Walecka, Advances of Nuclear Physics, vol. 16 (Plenum Press, New York, 1986).

[22] J. Schaffner, I.N. Mishustin, L.M. Satarov, H. Stöcker, and W. Greiner , Z. Phys. A341 (1991) 47.

[23] C.J. Horowitz and B.D. Serot, Nucl. Phys. A368 (1981) 503.

[24] J. Boguta, Phys. Lett. B106 (1981) 245.

[25] N.K. Glendenning, ApJ 293 (1985) 470.

[26] N.K. Glendenning, S.A. Moszkowski, Phys. Rev. Lett. 67 (1991) 2414.

[27] G.A. Lalazissis, J. König and P. Ring, Phys. Rev. C55 (1997) 540.

[28] S. Typel and H.H. Wolter, Nucl. Phys. A656 (1999) 331.

[29] S.S. Avancini. M.E. Bracco, M. Chiapparini and D.P. Menezes, J. Phys. G: Nucl. Part. Phys. 30 (2004) 27.

[30] J. Theis, G. Graebner, G. Buchwald, J. A. Maruhn, W. Greiner, H. Stöcker and J. Polonyi, Phys. Rev. D28 (1983) 2286.

[31] D.P. Menezes, C. Providência, M. Chiapparini, M. E. Bracco, A. Delfino, and M. Malheiro, Phys. Rev. C76 (2007) 064902.

[32] J. Schaffner-Bielich and A. Gal, Phys. Rev. C 62 (2000) 034311.

[33] J. Schaffner-Bielich, Phys. Rev. Lett. 89 (2002) 171101-1.

[34] E. Friedman, A. Gal, Phys. Rep. 452 (2007) 89.

[35] C.B. Dover and A. Gal, Progress in Particle and Nuclear Physics, vol. 12 (1984) 171.

[36] I.N. Mishustin, Sov. J. Nucl. Phys. 52 (1990) 722, Yad. Fiz. 52 (1990) 1135.

[37] W. Greiner and B. Mueller, Quantum Mechanics: Symmetries, 2nd edition (Spring-Verlag, Berlin Heildenberg, 1994).

[38] I. N. Mishustin et al, Phys. Rev. C71 (2001) 035201.

[39] P.K. Panda, M.E. Bracco, M. Chiapparini, E. Conte, and G. Krein, Phys. Rev. C65 065206.

[40] M. Nielsen, C. Providência and J. da Providência, Phys. Rev. C 47, 200 (1993).